Vacuum 156 (2018) 9–19

Contents lists available at ScienceDirect

Vacuum

journal homepage: www.elsevier.com/locate/vacuum

Magnetic field influence on ionization zones in high-power impulse Magnetron Sputtering

Priya Raman[a,*], Matthew Cheng[a], Justin Weberski[a], Wenyu Xu[a], Thomas Houlahan[b], Jose Rivera[b], Rui Su[b], Ivan Shchelkanov[a], David Ruzic[a]

[a] Center for Plasma Material Interactions, University of Illinois, Urbana, USA
[b] Laboratory for Optical Physics and Engineering, University of Illinois, Urbana, USA

ABSTRACT

High Power Pulsed Magnetron Sputtering (HPPMS) or High Power Impulse Magnetron Sputtering (HiPIMS) is a promising Ionized Physical Vapor Deposition (iPVD) technique that is capable of producing high quality, ultra-dense, wear-resistant, low-friction coatings with superior adhesion to the substrate. Despite the deposition of high quality films, HiPIMS suffer from lower deposition rates when compared to DC Magnetron Sputtering (dcMS). The cylindrically symmetric TriPack magnet pack which is the primary focus of this article has demonstrated increased deposition rates in HiPIMS compared to conventional magnet arrangement for the same average power. The observed difference in overall deposition rates, erosion area, voltage-current traces and pulsing parameters influence on deposition rates of TriPack from conventional magnet pack indicates that the plasma dynamics of TriPack is very different from the conventional magnet pack. In order to study the discharge dynamics of the cylindrically symmetric TriPack magnet pack, a gated ICCD camera was used to investigate the moving localized ionization zones in this magnet pack and conventional magnet pack for the same average power. Additionally, a simple HiPIMS ionization zone model was developed to predict the occurrence of ionization zones in TriPack and conventional magnetic field configurations under certain experimental/discharge conditions.

1. Introduction

HiPIMS plasma [1,2] is characterized by a high discharge current which generates plasma waves and instabilities that induces plasma flares [3], azimuthally symmetric particle jets [4] and self-organized patterns [5]. Plasma instability like the drifting ionization/"hot" zones/ Plasma spokes on HiPIMS plasma have been observed by many groups [6–9] around the world. These “plasma spokes” are also observed in dc magnetron discharges even at low target current densities and the shape of these spokes have a strong dependence on the strength of the magnetic field of the magnetron used [10].

Ehiasarian et al. [7] had reported plasma instabilities in HiPIMS discharges that include regions of bright and dark plasma arranged periodically along the race track region of a 50 mm titanium target and these dense plasma structures move anticlockwise in the ExB direction with linear velocities of 10–20 km/s. These drift wave instabilities under certain experimental conditions, saturate and form azimuthally periodic structures rotating between 100 and 200 kHz [7]. Anders et al. [11] found localized hot ionization zones drifting along the race track in the ExB direction with a velocity that is 10% of the electrons ExB drift velocity. The azimuthal velocity of these ionization zones was reported to be around 10^4 m/s and the azimuthal velocity of these ionization zones depends on the gas type and the target material.

Boeuf et al.’s PIC-MCC (Particle-In-Cell Monte Carlo Collisions) simulations [12] showed that the formation of plasma non-uniformities perpendicular to the magnetic field leads to anomalous transport across magnetic fields in Hall thrusters and cylindrical magnetrons. It was revealed from his 2D simulation work that the electron sheath next to the anode was unstable and transformed into rotating electron vortices at lower pressures whose time of evolution is much longer than the rotational period. At higher pressures, the plasma properties are not azimuthally symmetric and there is an abrupt azimuthal drop or spoke that defines separation between two plasma regions.

It was earlier thought that the ionization zones propagate at velocities between 10^3 m/s to 10^4 m/s in the ExB direction [7]. But Yang et al. [13] has observed that these ionization zones actually move in the ExB direction with velocities of 10^3–10^4 m/s in the case of higher discharge currents compared to velocities of 10^3 m/s in the negative ExB direction in the case of lower discharge currents. There have been several attempts by many research groups around the world to understand and explain the formation of ionization zones in HiPIMS discharges [7,8,14–18]. In one such attempt, Gallian et al. [14] developed a simplistic phenomenological model for a single rotating spoke by taking in to account certain chemical species and subjecting them to diffusion and drift processes that are typical to HiPIMS discharges. Their model helps to define a single rotating steady-state configuration

* Corresponding author.
E-mail address: raman6@illinois.edu (P. Raman).

https://doi.org/10.1016/j.vacuum.2018.07.008
Received 11 June 2018; Received in revised form 4 July 2018; Accepted 5 July 2018
Available online 06 July 2018

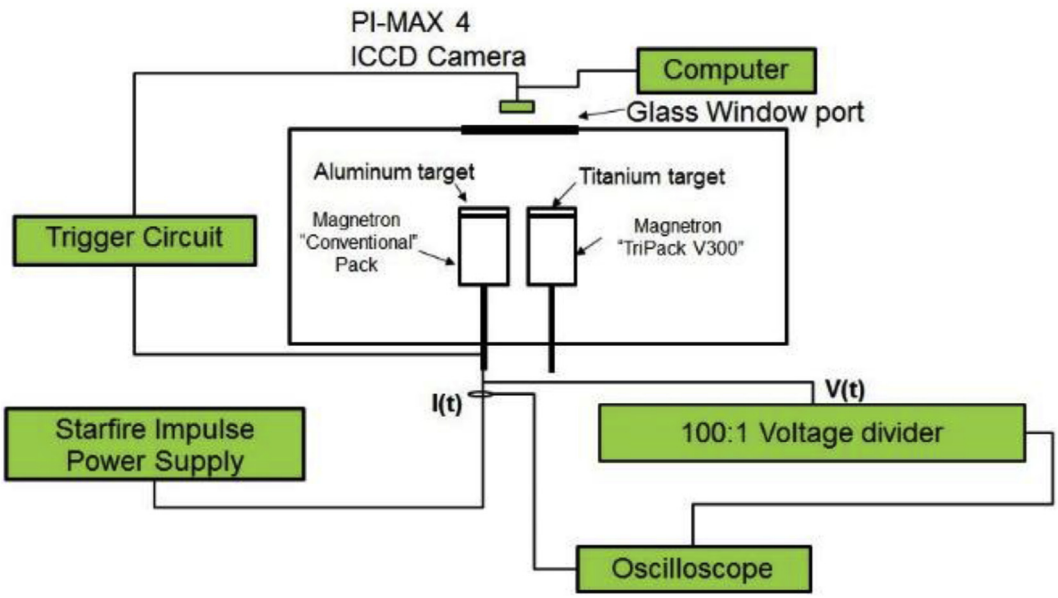

Fig. 1. Schematic of the ICCD camera set-up and the dual magnetron chamber.

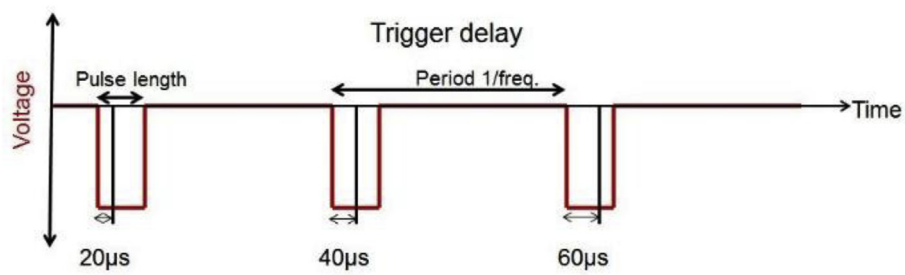

Fig. 2. Illustration of how the ICCD camera was triggered with respect to the HiPIMS voltage pulse using the external trigger circuit. The shutter was open for 10 ns?

Table 1a
ICCD camera experimental conditions.

Voltage	Average power (W)	HiPIMS pulse length (μs)	Trigger delay (μs)
650	250 500	50, 200, 250, 500	Every 20
950	250 500	50, 200, 250, 500	Every 20

Table 1b
Main experimental conditions.

	Conventional Magnet Pack	TriPack V300 Magnet Pack
Gas	Argon	Argon
Pressure	20mTorr	20mTorr
Power Supply	Starfire Impulse	Starfire Impulse
Target	Aluminum	Titanium

of the electron and neutral densities. In this work, a detailed study has been carried out to understand the occurrence of ionization zones in different magnetic field configurations and a "Critical Current Density Model" was developed to predict the formation of ionization zones in HiPIMS discharges. Based on previous studies, it was shown that the TriPack magnet pack was able to obtain higher deposition rates in HiPIMS compared to the conventional magnet pack [19]. There have been several publications in the past that show that lowering the magnetic field strength leads to higher deposition rates, due to a reduction in the metal ion "return effect" [20]. This is not the case for the TriPack V300, where the radial component of the magnetic field on the surface of the target is higher than the conventional pack. The race track area of the conventional pack is only 6 in^2, whereas the race track area of the TriPack V300 is ~8 in^2. The TriPack V300 race track area is 25% larger, but has much lower discharge current when compared with the conventional pack [19,21]. Both these observations combined do not support the simple explanation that higher race-track area gives higher deposition rates. The observed difference in deposition rates, erosion area, voltage-current traces and pulsing parameters influence on deposition rates of TriPack V300 from conventional magnet pack indicates that the plasma dynamics of this magnet pack is very different from the conventional magnet pack. Hence, in order to understand the discharge dynamics in this pack, ionization zone observation studies were carried out with the help of an ICCD camera. In this work, an ICCD camera was used to understand the behaviour of HiPIMS discharges in different magnetic field configurations.

2. Experimental set-up

All the experiments discussed in this work were carried out in the SHADE chamber. Sputtering high-purity atomic deposition experiment (SHADE) is a dual 10 cm diameter magnetron set-up (Fig. 1) for depositing thin films in an ultra-high vacuum (UHV) environment. In this work, two different magnet packs namely TriPack and conventional magnet pack were used. Starfire Impulse power supply (average power: 0–2 kW; maximum voltage: 1000 V; maximum current: 200 A; pulse length 5 μs–1 ms; frequency: 1 Hz–10 kHz) was used for igniting HiPIMS discharge [19,22]. The TriPack magnet pack will be referred to as

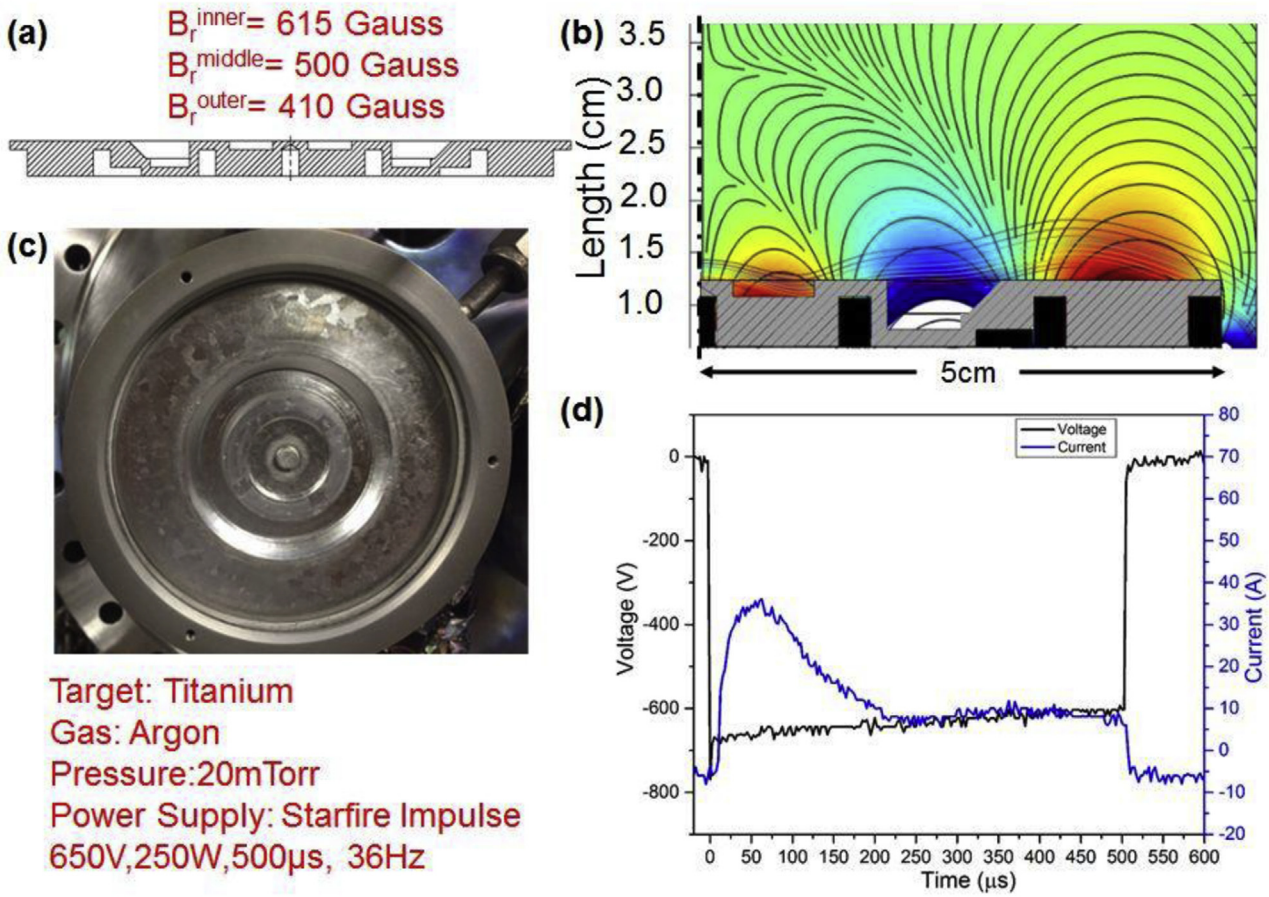

Fig. 3. (a) Side view of the TriPack V300 titanium target with the peak radial magnetic field values on the three race tracks, (b) Streamline plot of B_x and B_z components on the target surface simulated in COMSOL Multiphysics, (c) Photograph of the pre-eroded titanium target, (d) VI oscillogram for 500µs pulse width.

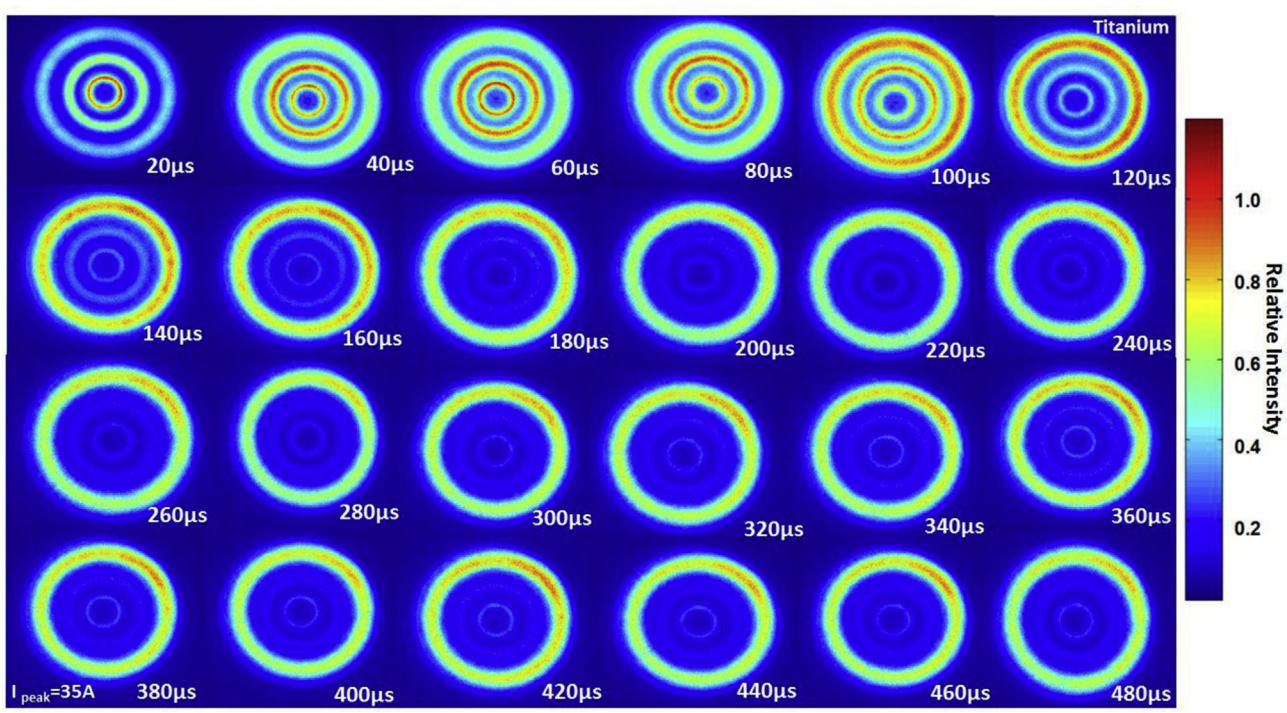

Fig. 4. ICCD images of TriPack V300 titanium HiPIMS discharge with timestamps for 500 µs, 650 V, 250 W and 20mTorr process conditions. For a 500µs HiPIMS pulse, pictures were taken at 20, 40 .....480 µs?as shown in this figure. The exposure time of these images are 10ns and the peak current density during this charge is 0.68 A/cm^2.

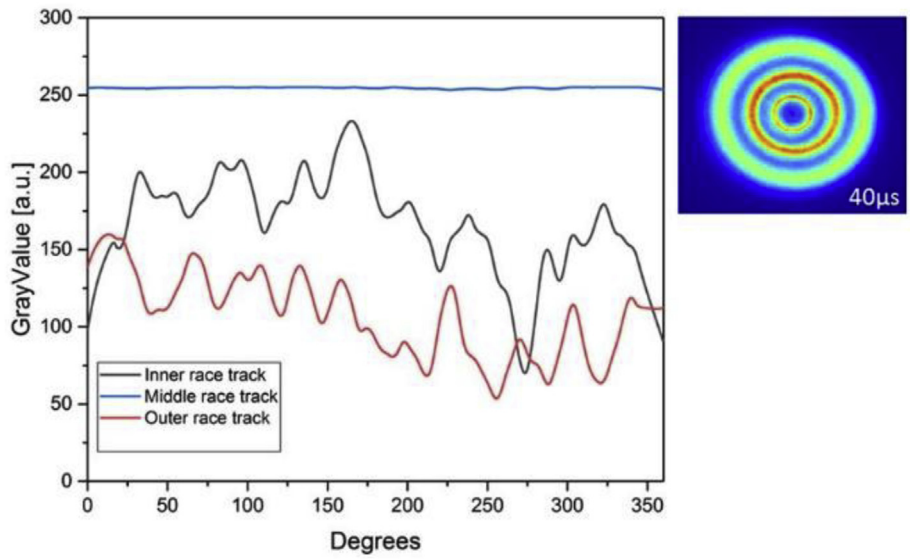

Fig. 5. Gray value profile of the image (at 40 µs) at which the peak current density was reached when all the three race tracks are operated simultaneously.

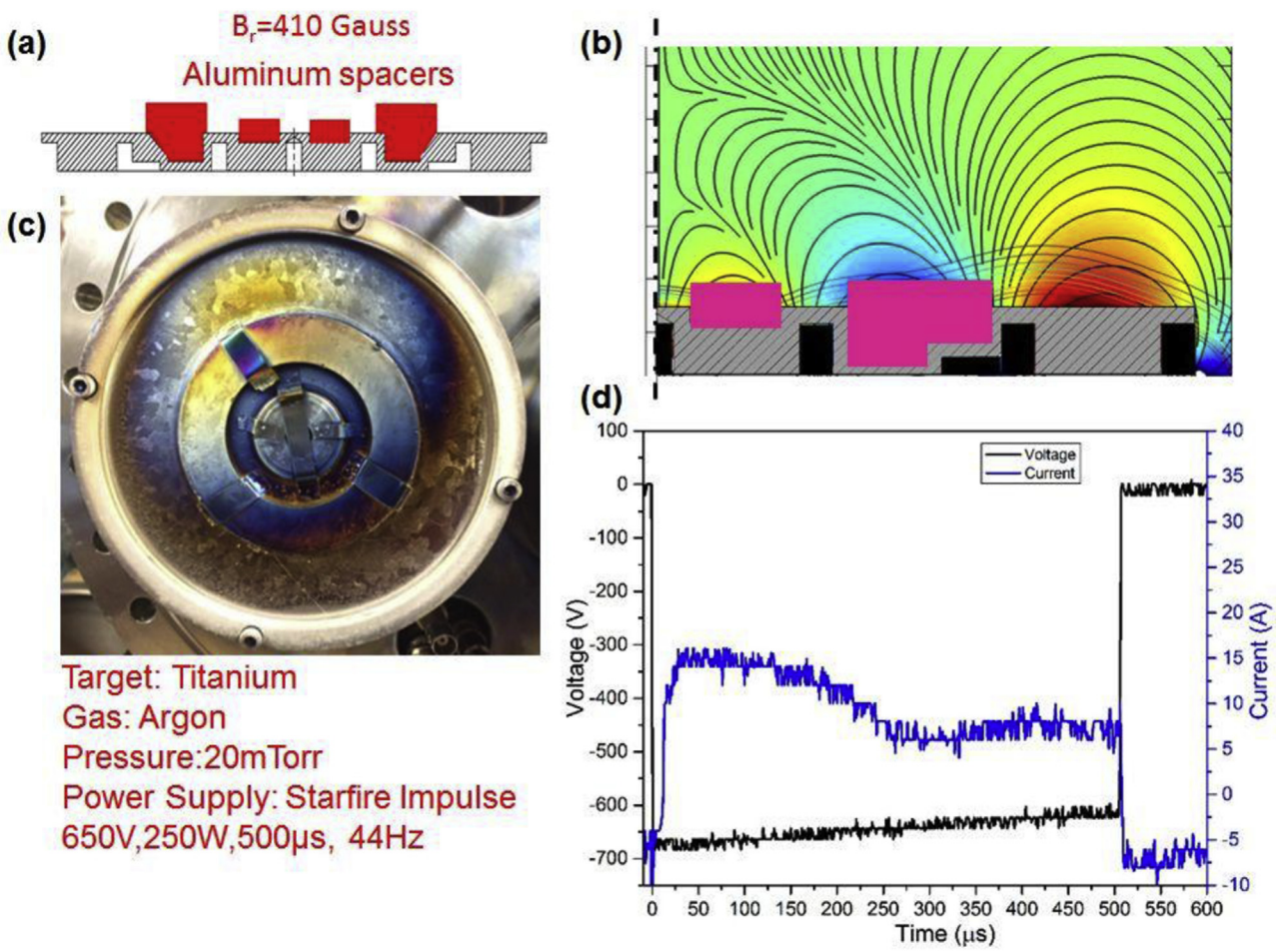

Fig. 6. (a) Side view of the TriPack V300 titanium target with the magnetic insert slots and aluminum spacers on the inner and middle race track, (b) Streamline plot of B_x and B_z components on the target surface simulated in COMSOL Multiphysics, (c) Photograph of the pre-eroded titanium target with aluminum spacers on the inner and middle race tracks, (d) VI oscillogram for 650 V, 250 W, 500 µs operating condition.

"TriPack V300" in the rest of this article. An ICCD camera was used in this work to capture the ionization zones in the HiPIMS discharge. A Princeton Instruments PI MAX-4 gated ICCD camera with an f = 70 mm (lens aperture of f/2.8) Nikon lens was used in this work. This camera contains a 1 Megapixel (1024 × 1024) array of square shaped detectors with an edge length of 12.8 µm. A custom external trigger circuit was built to trigger the camera based on the start of every HiPIMS voltage pulse. The ICCD camera was triggered once per pulse and the trigger

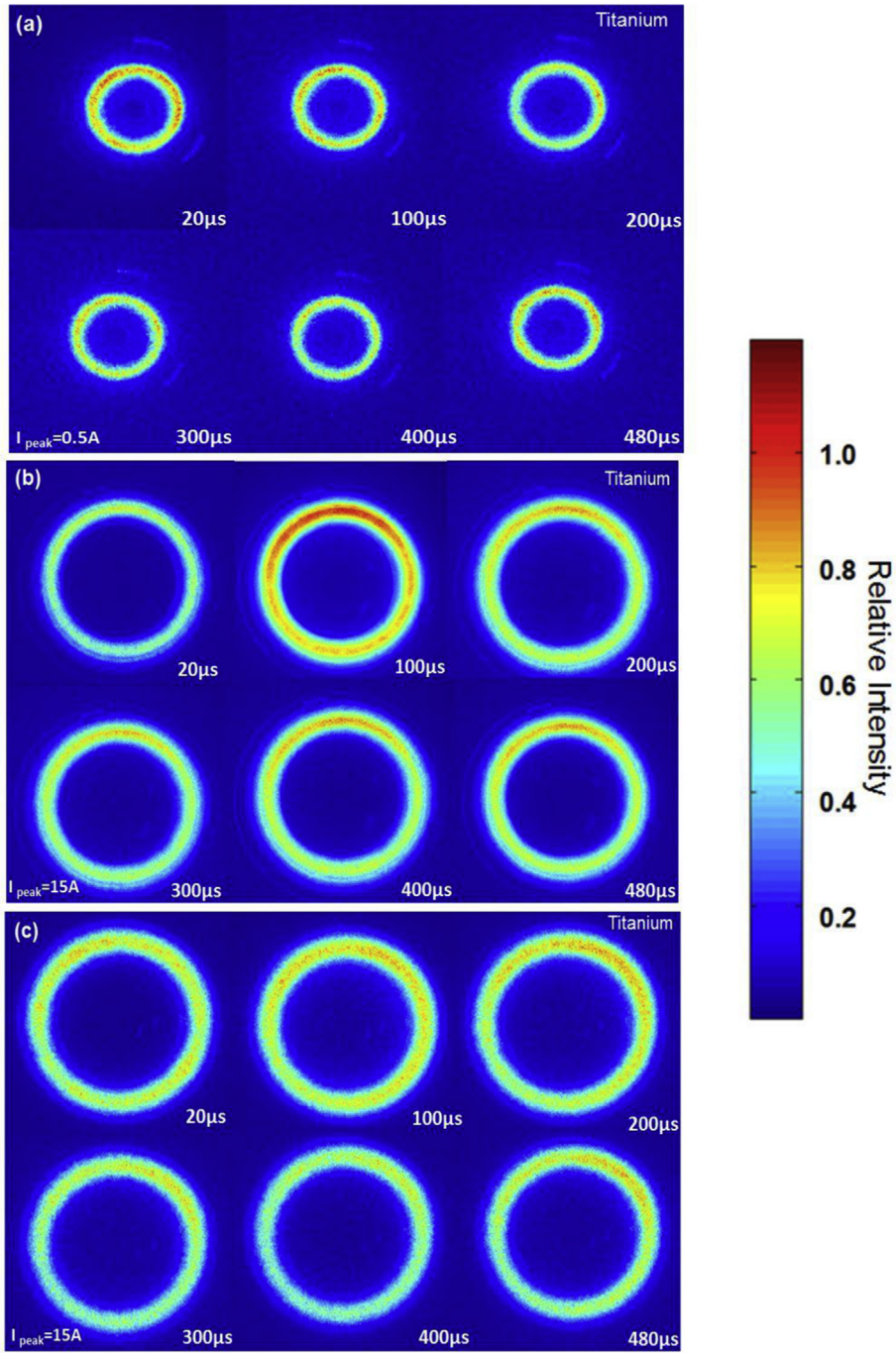

Fig. 7. ICCD images of the TriPack V300 titanium HiPIMS discharge on the (a) inner, (b) middle, and (c) outer race tracks, respectively, with timestamps. The discharge corresponds to 500 µs, 650 V, 250 W and 20mTorr process conditions. The exposure time of these images are 10ns and the corresponding peak current densities during each case is (a) 0.37 A/cm^2, (b) 1.26 A/cm^2, and (c) 0.39 A/cm^2.

time was every 20µs from the start of consecutive HiPIMS voltage pulses. For example, for a 500µs HiPIMS voltage pulse, the ICCD camera was triggered at 20, 40, 60 …. 480µs from the start of each consecutive HiPIMS voltage pulse. An illustration of how the camera was triggered is shown in Fig. 2. The gate width for these experiments was fixed at 10ns and all ICCD images shown in this work were taken from one shot and not an average over many pulses. Fig. 1 is the schematic of the ICCD camera set-up. Table 1 (a & b) summarizes the experimental conditions that were explored in full for this work. The results from the 650 V and 250 W average power experimental conditions will be the focus of the remainder of the discussion.

3. Results

In this work, two different TriPack V300 experiments were carried out. In the first experiment, all three race tracks were ignited simultaneously under normal TriPack V300 operation. For comparison purposes, regular ignition/operation of this magnet pack will be referred to as simultaneous ignition of three racks in this article. In the second experiment, the discharge was ignited on one race track at a time to understand the interactions between the race tracks. A titanium target was used for all the TriPack V300 magnet pack experiments and an aluminum target was used for all the conventional magnet pack experiments.

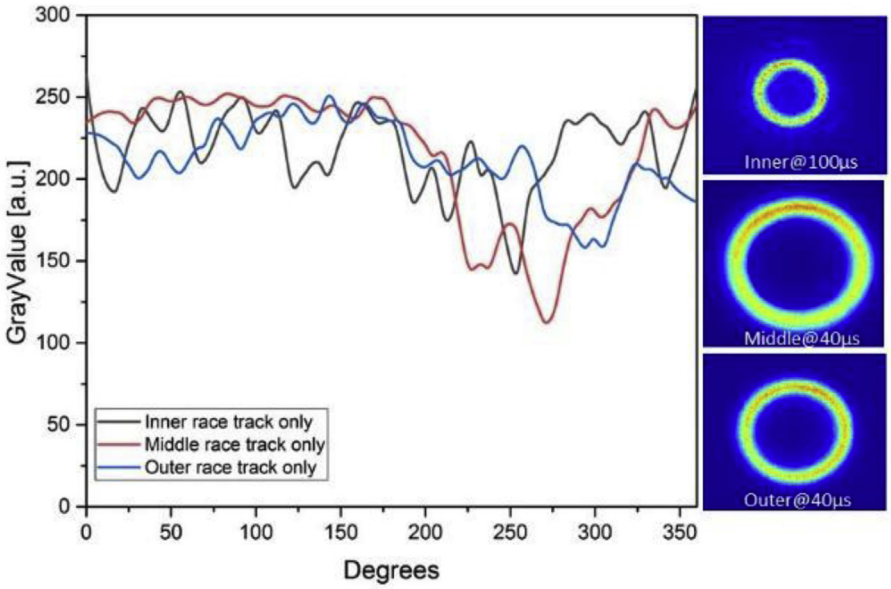

Fig. 8. Gray value profile of the images at which the peak current density was reached when the three race tracks are operated individually. Peak current density for inner, middle and out race tracks were reached at 100 µs, 40 µs and 40 µs respectively.

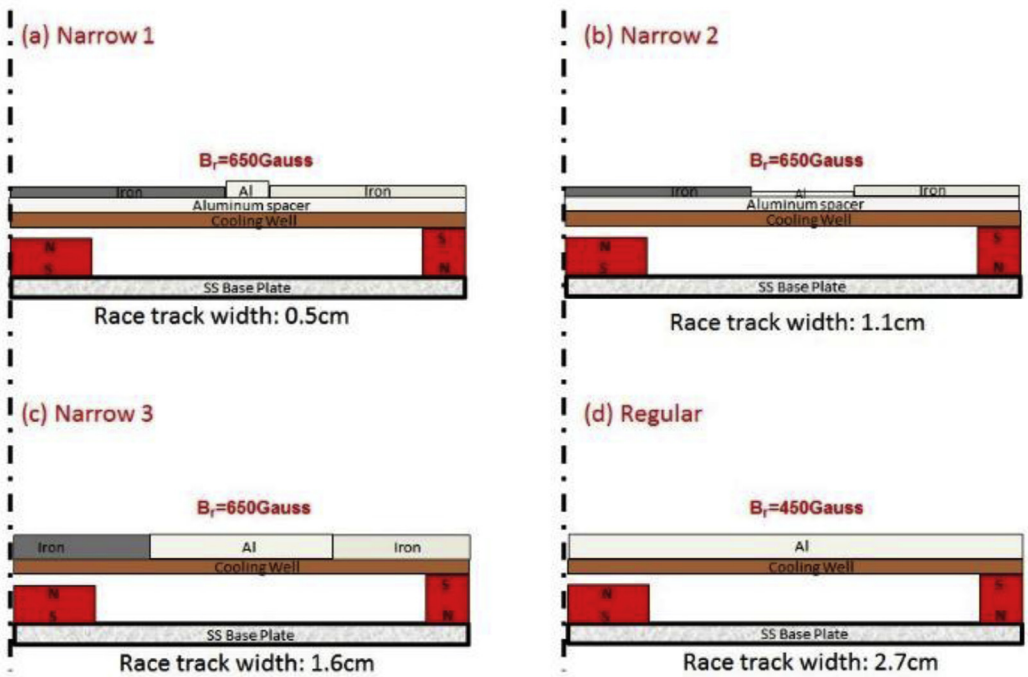

Fig. 9. Schematic of the different race track width configurations: (a) Narrow 1, (b) Narrow 2, (c) Narrow 3, and (4) Regular.

3.1. ICCD study of ignition on all the three race tracks simultaneously

The experimental and magnetic field details for simultaneous operation of all the three race tracks are shown in Fig. 3. Fig. 3(a) shows the side view of the pre-eroded TriPack V300 target with the slots for magnetic inserts [19], Fig. 3(b) shows the streamline plot of the B_x and B_z components on the pre-eroded target surface, Fig. 3(c) is the photograph of the TriPack V300 pre-eroded target, and Fig. 3(d) is the HiPIMS VI oscillogram that corresponds to a HiPIMS discharge with a pulse width of 500 µs. Fig. 4 shows the ICCD camera results for this case.

The scale bar on the ICCD images shows the relative intensities, where blue represents the lowest intensity and red represents the highest intensity. It can be observed in Fig. 4 that in the 500µs case, initially there is an intense discharge in the inner race track compared to the middle race track and the outer race track looks very faint. As the discharge progresses, the relative intensities change substantially. At 100 µs, the middle and outer tracks look more intense than the inner race track. As time progresses, the inner and middle tracks fade away while the outer track remains bright until the end of the discharge. The plasma around the race tracks remains homogeneous without any ionization zones/plasma spokes and the peak current was around 35A during this discharge. Fig. 5 shows the intensity profile along the race tracks in the azimuthal direction from the image at which the peak current density is reached. The intensity profile was obtained using ImageJ and the Oval Profile plugin. Presence of ionization zones in the

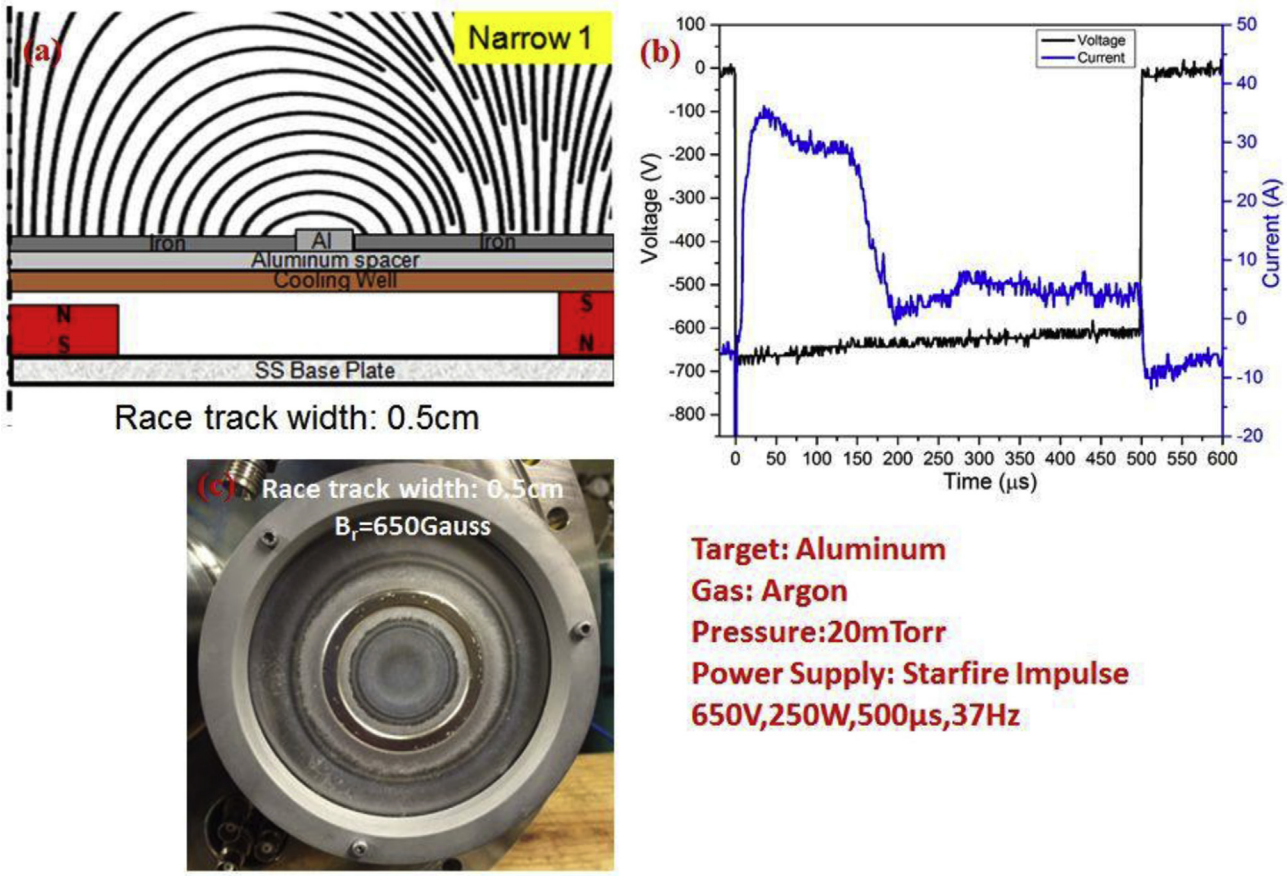

Fig. 10. (a) Schematic of Narrow 1 configuration that corresponds to a race track width of 0.5 cm at B_r = 650Gauss, (b) VI oscillogram corresponding to Fig. 9 (a), (c) Photograph of the aluminum target placed between iron spacers.

intensity profile is characterized by the modes (sharp, narrow dip in the profile plot) and clearly Fig. 5 indicates the absence of ionization zones when all the three race tracks are operated simultaneously. Intensity along the race tracks were analysed for all the timestamps but only the timestamps at which the peak current density was reached is presented. The intensity profile from all the timestamps indicated the absence of ionization zones. The y value indicated in the intensity plot is a number used to indicate the intensity/amount of gray in a particular pixel of an image on a scale from white to black with 0% being black and 100% being gray.

3.2. ICCD study of ignition on one race track at a time

In order to understand if there are plasma interactions between the race tracks, HiPIMS discharge was ignited on a single race track at a time. This was achieved by inserting thick aluminum spacers on specific race tracks. The spacers reduced the field to the point where there was not enough confinement to ignite a plasma. The aluminum spacers were spot welded using stainless shim stock on specific race tracks to avoid a discharge on that track. The magnetic field strength on the top of the aluminum spacers (thick targets) were less than 50 Gauss. For example, to achieve discharge on the inner track, aluminum spacers were placed on the middle and outer race tracks. Similar discharges were achieved on the middle and outer race tracks by placing aluminum spacers on the other race tracks in each respective case. As an example, details of the outer race track experiment are shown in Fig. 6. Fig. 7 (a, b, &c) shows the ICCD images from each of the individual race track discharge experiments. It can be observed in Fig. 7(a) that the discharge in the inner track was homogeneous without any “ionization zones'/plasma spokes. The intensity remained more or less the same throughout the discharge. Fig. 7(b) shows the discharge on the middle race track. At 20 μs from the start of the HiPIMS discharge, the plasma on the middle race track is faint which then becomes very bright at 100 μs? The discharge on the middle race track was homogeneous with no ionization zones/plasma spokes. The discharge on the outer race track (shown in Fig. 7(c)) is also homogenous throughout the HiPIMS pulse.

The main observation from all these TriPack V300 experiments is that the plasma looks homogeneous without ionization zone/plasma spokes (Fig. 8) even with discharge on only one race track at a time. The intensity profile analysis from all the timestamps indicated the absence of ionization zones in each of the individual cases (Inner, middle and outer race tracks). While there is some variation of light around the ring, the position around 250° is slightly lower due to uneven pre-erosion, not a rotating ionization zone.

3.3. Influence of race track width on the formation of ionization zones

All the ICCD observations from the study of the TriPack V300 leads to the question of whether or not the ionization zones/plasma spokes formation are related to the race track widths (race track width dictates the race track area) because the race track widths (race track area) in the TriPack V300 are not the same for all three race tracks. In order to investigate the effect of race track widths on the ionization zone/plasma spokes, a series of ICCD experiments were conducted where, the race track widths of the target (aluminum in this case) on the conventional magnet pack were varied but the magnitude of the radial magnetic field was kept constant at 650Gauss. This was achieved by carefully placing iron spacers between the magnetron target (Fig. 9) to shape the magnetic field lines and their magnitude on the top of the target. The dimensions of the target and the iron spacers are critical in

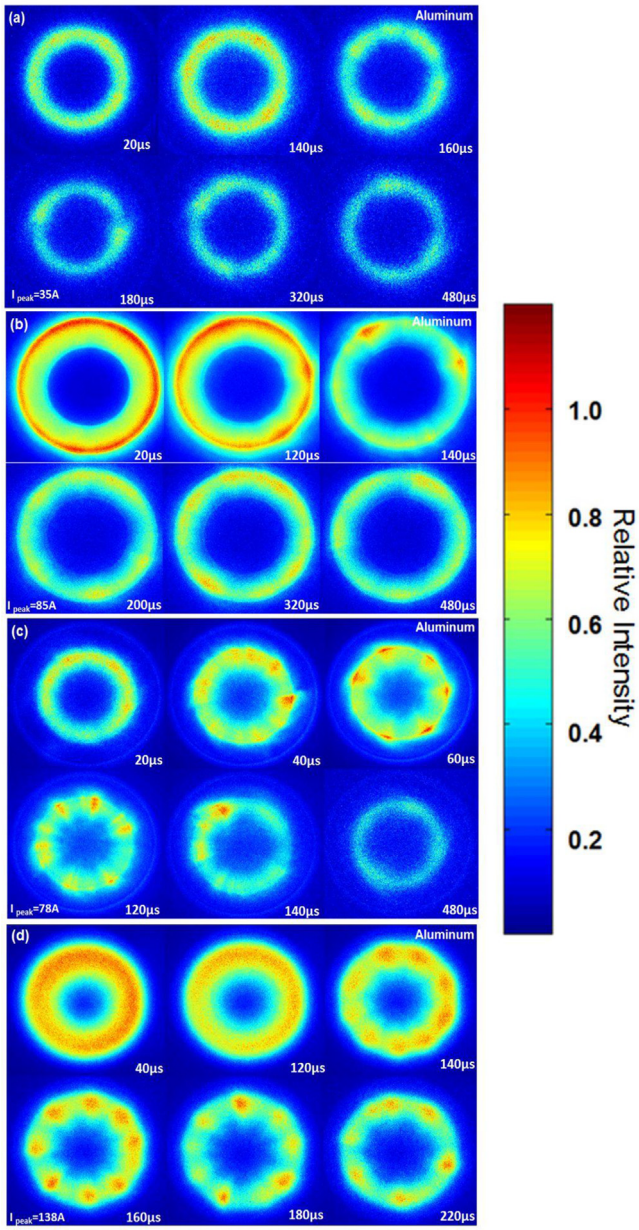

Fig. 11. ICCD images from (a) Narrow 1, (b) Narrow 2, (c) Narrow 3, and (d) Regular standard magnet pack configurations during HiPIMS discharge with times. Images (a), (b), and (c) discharges correspond to 500 µs, 650 V, 250 W and 20mTorr process conditions and (d) corresponds to 250 µs, 650 V, 250 W, and 20mTorr process conditions. The exposure time of all images is 10ns and the corresponding peak current densities during each case is (a) 4.78 A/cm^2, (b) 5.41 A/cm^2, (c) 3.50 A/cm^2, and (d) 3.90 A/cm^2.

achieving the right magnetic field values. Hence, the set-up was simulated in COMSOL Multiphysics to get the accurate dimensions of the target and the iron spacers.

Four different race tracks widths (0.5 cm, 1.1 cm, 1.6 cm at B_r = 650Gauss and 2.7 cm at B_r = 450Gauss) were studied and aluminum was chosen as the target material due to its ease of machining. In all these experiments, the ICCD camera was triggered every 20 µs from the start of the consecutive pulses. Not all ICCD images from various times are shown, only the important ones. As an example, Fig. 10 shows the details of the "Narrow 1" configuration with the corresponding VI trace. The HiPIMS operating parameters and the argon pressure was kept constant at 20mTorr to be consistent with the TriPack V300 titanium experiments.

It can be observed from Fig. 11(a) that for the "Narrow 1" (0.5 cm wide race track) case, at 20 µs from the start of the discharge, the plasma looks more or less homogeneous and at 140 µs, plasma contraction can be seen. The ionization zones/plasma spokes start to appear at about 160 µs and lasts till the end of the pulse (480 µs). The peak discharge current during this experiment is ~35A.

Fig. 11(b) shows the ICCD images obtained from the "Narrow 2" configuration. In this case, at 20 µs from the start of the discharge, the plasma is very intense and homogenous and at 140 µs, distinct plasma spokes can be observed, and they last till the end of the pulse (480 µs). The peak HiPIMS discharge current during this experiment is ~85A.

The ICCD images from the "Narrow 3" configuration (Fig. 11(c)) indicate that initially at 20 µs, the plasma is homogeneous and distinct plasma spokes starts to appear at 40 µs from the start of the discharge. The number of spokes decreases as time progresses and they eventually fade away at the end of the pulse (480 µs).

In the "Regular" case, the race track width was 2.7 cm but the magnitude of the radial magnetic field is 450Gauss. Therefore, in this case the race track is physically wider but has a lower radial magnetic field compared to the previous cases. This case is called "Regular" because this set-up is the same as the conventional magnet pack set-up with a 0.6 cm thick aluminum target. In this experiment, the pulse width was set at 250 µs instead of 500 µs because of the process constraints in achieving the same average power (250 W) with at a fixed voltage (650 V). It can be observed from the corresponding ICCD images (Fig. 11(d)) that initially at 20 µs from the start of the discharge, the plasma looks intense and homogeneous. At 140 µs, distinct plasma spokes appears and the number of spokes is reduced as time progresses. The plasma spokes lasts until the end of the pulse (250 µs). The peak HiPIMS current during this case is ~138A. Ionization zones were observed (Figs. 12 and 13) in all the different race track width cases considered in our experiments. Fig. 12 is the intensity profile along the race tracks in the azimuthal direction from the image at which the peak current density is reached and Fig. 13 is the intensity profile along the race tracks in the azimuthal direction from the image at which the spokes were prominent for the different race track width experiments. Spokes/modes are not very prominent is Narrow 2 and Regular cases in Fig. 12 but in Fig. 13 they are prominent. This clearly indicates that spokes/modes can occur on or after peak current density has passed.

Some of the main observations from the variable race track width experiments are as follows:

1. As the width of the race track decreases, the time for the plasma spokes to form increases for a set voltage and average power.
2. As the magnitude of the radial magnetic field (B_r) decreases, the time for the plasma spokes to form increases for a set voltage and average power.

4. Discussion

It is clear from all the above observations that the physics of HiPIMS is very complex in nature because the plasma evolves in time and volume during the sputtering process. This means the composition of the plasma, the electron temperatures, the ambient magnetic field and the spatial electric potential changes over time [23]. Based on the above experimental observations, a simple "Critical Current Density Model" was developed to predict the critical current density needed to create ionization zones for different magnetic field configurations in HiPIMS. Basically, the hypothesis is that an isolated hot spot only appears if the conditions are such that all of the gas in a particular location is ionized.

4.1. "Critical Current Density Model"

The ionization rate for a gas in a plasma is given by:

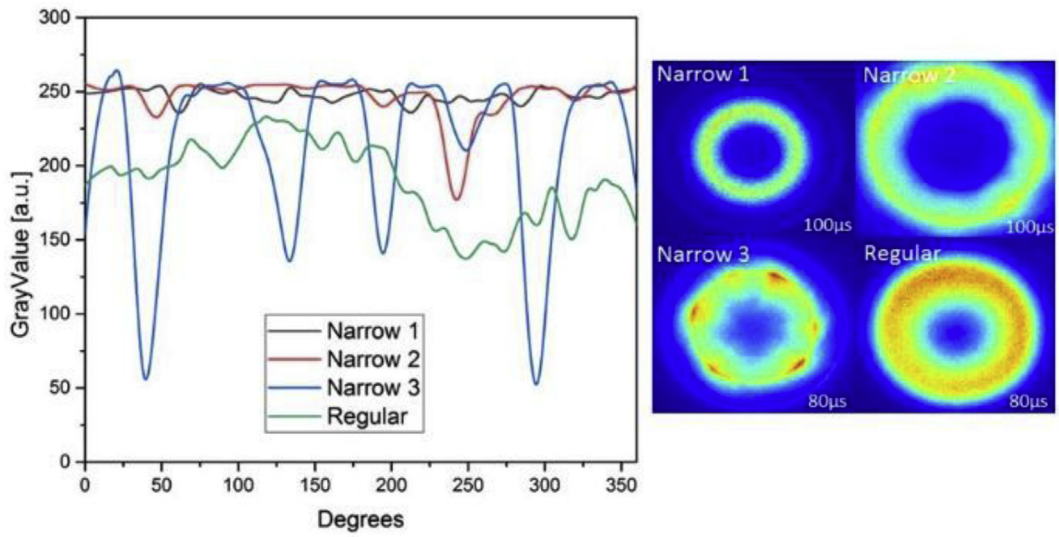

Fig. 12. Gray value profile of the images at which the peak current density was reached from different rack width experiments. Peak current density for Narrow 1, Narrow 2, Narrow 3 and Regular cases were reached at 100 µs, 100 µs, 80 µs and 80 µs respectively.

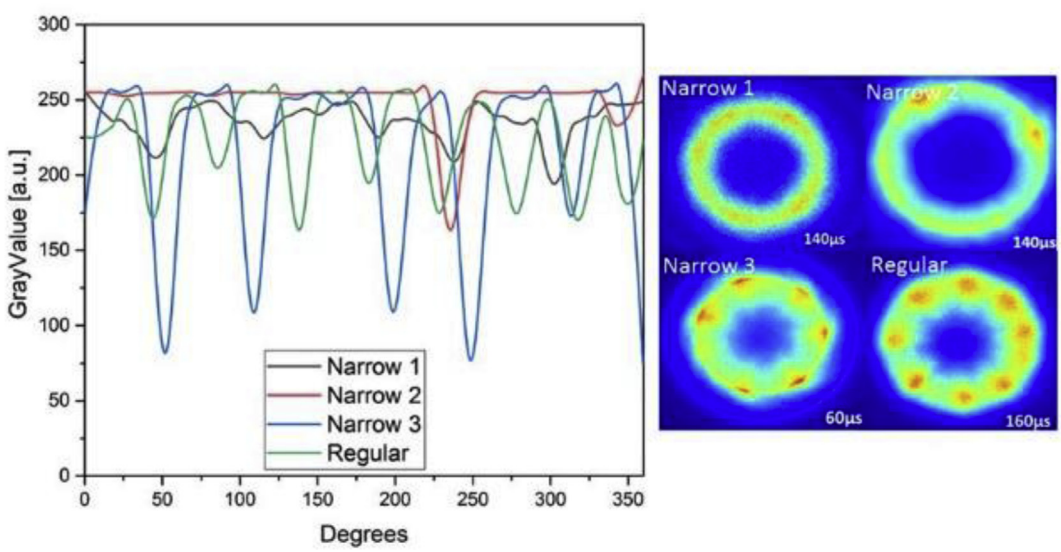

Fig. 13. Gray value profile of the images from the different rack width experiments when the ionization zones are prominent. The ionization zones were prominent for Narrow 1, Narrow 2, Narrow 3 and Regular cases at 140 µs, 140 µs, 60 µs and 160 µs respectively.

Table 2
Various parameters used in the calculation of critical current density for conventional and TriPack V300.

Parameter	Conventional Magnet Pack	TriPack V300 Magnet Pack
Race track area in cm^2	38.7	51.6
Speed of sputtered atoms (V) in m/s	3782	3782
Sputter yield (Y)	1.267	1.267
Ionization probability in the highly confined plasma (α)	0.818 [19]	0.022 [19]
Gas refill time (τ) in s	0.00004	0.000016
k_{iz} in m^3/s	2.65E-14	2.65E-14
Critical Current Density ($A*cm^{-2}$)	0.06	5.1

$$\frac{dn_+}{dt} = n_e n_g k_{iz} \tag{1}$$

where n_+ is density of ionized gas in the ionization zone. The rate at which the gas is ionized depends on the electron density (n_e), neutral gas density (n_g), rate coefficient for electron impact ionization of argon gas where $k_{iz} = \sigma\upsilon$. σ is the electron-atom ionization cross-section and υ is the average velocity of the electrons. By integrating equation (1), the density of the ionized gas can be written as

$$n_+ = n_e n_g \tau k_{iz} \tag{2}$$

where τ is the neutral gas refill time, which is the time for new gas to diffuse into the ionization zone. Since it is known from the literature [3,11,24] that ionization zones appears if all the gas is ionized at a given location, a critical condition for ionization zones to form can be determined by letting $n_+ = n_g$.

So,

$$1 = n_e \tau k_{iz} \tag{3}$$

The electron density (equation (4)) can be approximated in terms of current density (J), sputter yield (Y), ionization probability in the plasma (α) [21,22], gas refill time (τ), the speed of sputtered atoms (V) and k_{iz} . The ionization probability (α) is different for conventional and

Table 3
Experimental target density and calculated critical target density for conventional and TriPack V300.

Magnet Pack	Experimental target current density (A/cm^2)	Theoretical critical current density (A/cm^2)
Conventional	3.9 ± 0.4	0.060 ± 0.005
TriPack V300	0.23 ± 0.02	5.1 ± 1.5

TriPack V300 magnet packs, and details of how it was calculated can be found in Ref. [22].

$$n_e = n_m * \alpha = JY\alpha\frac{1}{V} \tag{4}$$

where n_m is the density of sputtered atom. Substituting equation (3) in equation (4) leads to equation (5).

$$1 = \quad JY\alpha\frac{1}{V}\tau k_{iz} \tag{5}$$

Equation (5) is the condition for ionization zones to occur. The equation for determining the critical current density for ionization zones to appear can be written as

$$J_{critical} = \frac{V}{Y\alpha\tau k_{iz}} \tag{6}$$

If the experimental target current density (peak current density) is above the critical current density calculated using the above equation (Equation (6)), the ionization zones appear. The above equation (Equation (6))/model is applicable only for high-current HiPIMS plasma and not for low-current dcMS plasma.

By substituting the appropriate values on the RHS of equation (6), critical current densities for conventional pack and TriPack V300 are calculated to be $J^{con}_{critical} = 0.06Acm^{-2}$ and $J^{tri}_{critical} = 5.1Acm^{-2}$. Table 2 summarizes the various parameters used in the calculation of critical current density for conventional and TriPack V300 for an aluminum target. The gas refill time is shorter for the TriPack V300 because its race tracks are narrower.

Table 3 shows the comparison of experimental target density and calculated critical current density for both the magnet packs. The critical density for ionization zones to occur in the TriPack V300 is much higher than the conventional pack because of its lower α and smaller τ compared to the conventional pack. The ratio of the critical densities of the two magnet packs is

$$\frac{J^{con}_{critical}}{J^{tri}_{critical}} = 0.010 \tag{7}$$

The value of critical density in the TriPack V300 is much higher compared to the conventional pack. It can be observed from Table 3 that the experimental target current density of the TriPack V300 is more than an order of magnitude below the threshold to form ionization zones. The target current density is the ratio of peak target current to the race track area. Hence, no ionization zones were observed during TriPack V300 operation. On the other hand, the current density of the conventional pack is around 65 times larger than the critical density required for the ionization zones to be formed. Therefore, ionization zones should be observed which is in agreement with the experimental observation in the previous results section.

In order to validate this "Critical Current Density Model", critical current densities were calculated for other's work from the literature and were compared to their measured target current densities to predict the formation of ionization zones. The work of Yang et al. [25] was chosen because the experimental conditions and ICCD ionization zone images were available in their publication. Table 3 shows the comparison of experimental target densities and calculated critical current densities for Yang et al. [25], TriPack V300 and conventional pack. It can be seen from Table 4 that ionization zones were observed only when the critical densities were above the measured target current densities. The data from Yang et al. [25] agrees well with the "Critical Current Density Model". The "?" in Table 4 indicates the anomalies observed by Yang et al. and the "Critical Current Density Model". According to the "Critical Current Density Model", ionization zones have to be observed in the two cases indicated by a "?". But Yang et al. [25] does not observe ionization zones in those cases (copper target above 300A peak currents) and the discharge becomes homogeneous after a certain peak current (300A) only in the case of copper target. Hence, this is considered an anomaly and more detailed experimental/modelling efforts have to be undertaken to explain this observation in a copper target.

Table 5 compares the arc counts per minute obtained from conventional magnet pack and TriPack V300 magnet pack during HiPIMS discharge with an aluminum target at 20mTorr. It can be observed from Table 5 that at an average power of 500 W, the arc rate of TriPack V300

Table 4
"Critical Current Density Model" applied to other's work from the literature.

Source	Target	Voltage (V)	Peak Current (A)	Target Current Density (A*cm^{-2})	Critical Current Density (A*cm^{-2})	Ionization Zones Observed
Yang et al. [25]	Copper	550	0.2	0.01	0.03	No
			40	2		Yes
			100	5		Yes
			200	10		Yes
			300	15		?
			400	20		?
	Niobium	485	0.2	0.01	0.13	No
			40	2		Yes
			100	5		Yes
			200	10		Yes
			300	15		Yes
			400	20		Yes
	Titanium	500	0.2	0.01	0.14	No
			40	2		Yes
			100	5		Yes
			200	10		Yes
			300	15		Yes
			400	20		Yes
Conventional Pack (This work)	Aluminum	850	150	3.88	0.06	Yes
TriPack V300 (This work)	Aluminum	850	12	0.23	5.12	No
	Titanium	650	40	0.78	8.14	No
		950	59	1.14	6.35	No

Table 5
Arc rate of the TriPack V300 compared to the conventional magnet pack during HiPIMS discharge with an aluminum target at 20mTorr.

Average Power (W)	Magnet Pack	Arc counts/minute
500	Conventional	18
	TriPack V300	3

is about 6 times lower than conventional magnet pack. The reduction in arc rate may be attributed to the absence of ionization zones in TriPack V300.

5. Conclusion

The "ionization zones" were not observed in the TriPack V300 and the plasma was homogeneous on all the three race tracks whereas in the conventional pack, "ionization zones" were observed for the same average power. The "ionization zones" were not observed in TriPack V300 even with HiPIMS discharge on only a single race track. It was observed that the time for ionization zones to form increases when the race track becomes narrower and the strength of the radial magnetic field decreases for the same average power. Fewer number of arcs were observed in the TriPack V300 operation compared to the conventional magnet pack for the same average power. A simple "Critical Current Density Model" was developed to predict the threshold current density required for the formation of ionization zones for different magnetic field configurations in HiPIMS. The developed model agrees with the experimental data under certain experimental/discharge conditions.

Acknowledgements

This research was funded by the NSF Center for Lasers and Plasmas for Advanced Manufacturing under the I/UCRC program grant number 15-40030. This work was carried out in part in the Frederick Seitz Materials Research Laboratory Central Research Facilities and Visualization Laboratory at Beckman Institute in University of Illinois.

References

[1] D.V. Mozgrin, I. Fetisov, G. Khodachenko, High-current low-pressure quasi-stationary discharge in a magnetic field: experimental research, Plasma Phys. Rep. 21 (1995) 400–409.
[2] D. Lundin, K. Sarakinos, An introduction to thin film processing using high-power impulse magnetron sputtering, J. Mater. Res. 27 (2012) 780–792.
[3] P.A. Ni, C. Hornschuch, M. Panjan, A. Anders, Plasma flares in high power impulse magnetron sputtering, Appl. Phys. Lett. 101 (2012) 224102.
[4] M. Panjan, R. Franz, A. Anders, Asymmetric particle fluxes from drifting ionization zones in sputtering magnetrons, Plasma Sources Sci. Technol. 23 (2014) 025007.
[5] N. Brenning, D. Lundin, T. Minea, C. Costin, C. Vitelaru, Spokes and charged particle transport in HiPIMS magnetrons, J. Phys. Appl. Phys. 46 (2013) 084005.
[6] A. Kozyrev, N. Sochugov, K. Oskomov, A. Zakharov, A. Odivanova, Optical studies of plasma inhomogeneities in a high-current pulsed magnetron discharge, Plasma Phys. Rep. 37 (2011) 621–627.
[7] A. Ehiasarian, A. Hecimovic, T. De Los Arcos, R. New, V. Schulz-Von Der Gathen, M. Böke, J. Winter, High power impulse magnetron sputtering discharges: instabilities and plasma self-organization, Appl. Phys. Lett. 100 (2012) 114101.
[8] A. Anders, M. Panjan, R. Franz, J. Andersson, P. Ni, Drifting potential humps in ionization zones: the "propeller blades" of high power impulse magnetron sputtering, Appl. Phys. Lett. 103 (2013) 144103.
[9] J. Winter, A. Hecimovic, T. De los Arcos, M. Böke, V. Schulz-von der Gathen, Instabilities in high-power impulse magnetron plasmas: from stochasticity to periodicity, J. Phys. Appl. Phys. 46 (2013) 084007.
[10] M. Panjan, S. Loquai, J.E. Klemberg-Sapieha, L. Martinu, Non-uniform plasma distribution in dc magnetron sputtering: origin, shape and structuring of spokes, Plasma Sources Sci. Technol. 24 (2015) 065010.
[11] A. Anders, P. Ni, A. Rauch, Drifting localization of ionization runaway: unraveling the nature of anomalous transport in high power impulse magnetron sputtering, J. Appl. Phys. 111 (2012) 053304.
[12] J.-P. Boeuf, Rotating structures in low temperature magnetized plasmas—insight from particle simulations, Frontiers in Physics 2 (2014) 74.
[13] Y. Yang, J. Liu, L. Liu, A. Anders, Propagation direction reversal of ionization zones in the transition between high and low current magnetron sputtering, Appl. Phys. Lett. 105 (2014) 254101.
[14] S. Gallian, W. Hitchon, D. Eremin, T. Mussenbrock, R. Brinkmann, A phenomenological model for the description of rotating spokes in HiPIMS discharges, Plasma Sources Sci. Technol. 22 (2013) 055012.
[15] A. Hecimovic, Anomalous cross-B field transport and spokes in HiPIMS plasma, J. Phys. Appl. Phys. 49 (2016) 18LT01.
[16] A. Pflug, M. Siemers, T. Melzig, L. Schaefer, G. Bräuer, Simulation of linear magnetron discharges in 2D and 3D, Surf. Coating. Technol. 260 (2014) 411–416.
[17] C. Maszl, W. Breilmann, J. Benedikt, A. von Keudell, Origin of the energetic ions at the substrate generated during high power pulsed magnetron sputtering of titanium, J. Phys. Appl. Phys. 47 (2014) 224002.
[18] S. Tsikata, T. Minea, Modulated electron cyclotron drift instability in a high-power pulsed magnetron discharge, Phys. Rev. Lett. 114 (2015) 185001.
[19] P. Raman, I. Shchelkanov, J. McLain, M. Cheng, D. Ruzic, I. Haehnlein, B. Jurczyk, R. Stubbers, S. Armstrong, High deposition rate symmetric magnet pack for high power pulsed magnetron sputtering, Surf. Coating. Technol. 293 (2016) 10–15.
[20] A. Mishra, P. Kelly, J. Bradley, The evolution of the plasma potential in a HiPIMS discharge and its relationship to deposition rate, Plasma Sources Sci. Technol. 19 (2010) 045014.
[21] P. Raman, Magnetic Field Optimization for High Power Impulse Magnetron Sputtering, University of Illinois at Urbana-Champaign, 2016.
[22] P. Raman, J. Weberski, M. Cheng, I. Shchelkanov, D.N. Ruzic, A high power impulse magnetron sputtering model to explain high deposition rate magnetic field configurations, J. Appl. Phys. 120 (2016) 163301.
[23] M. Panjan, A. Anders, Plasma potential of a moving ionization zone in DC magnetron sputtering, J. Appl. Phys. 121 (2017) 063302.
[24] A. Anders, Self-organization and self-limitation in high power impulse magnetron sputtering, Appl. Phys. Lett. 100 (2012) 224104.
[25] Y. Yang, K. Tanaka, J. Liu, A. Anders, Ion energies in high power impulse magnetron sputtering with and without localized ionization zones, Appl. Phys. Lett. 106 (2015) 124102.